3D drift correction for super-resolution imaging with a single laser light

YUNZE LI,[1,†] YINGCHUAN HE,[1,†] KE FANG,[1] LULU ZHOU,[1] ZHEN WANG,[1] WEI SHI,[1,*] AND YIMING LI[1,*]

[1]*Department of Biomedical Engineering, Southern University of Science and Technology, Shenzhen 518055, China*
[†]*The authors contributed equally to this work.*
[*]*Corresponding authors: shiw@mail.sustech.edu.cn and liym2019@sustech.edu.cn*

Received XX Month XXXX; revised XX Month, XXXX; accepted XX Month XXXX; posted XX Month XXXX (Doc. ID XXXXX); published XX Month XXXX

Single-molecule localization microscopy (SMLM) enables three-dimensional (3D) super-resolution imaging of nanoscale structures within biological samples. However, prolonged acquisition introduces drift between the sample and the imaging system, resulting in artifacts in the reconstructed super-resolution image. Here, we present a novel 3D drift correction method that utilizes both the reflected and scattered light from the sample. Our method employs the reflected light of a near-infrared (NIR) laser for focus stabilization while synchronously capturing speckle images to estimate lateral drift. This approach combines high-precision active compensation in the axial direction with lateral post-processing compensation, achieving the abilities of the 3D drift correction with a single laser light. Compared to the popular localization events-based cross-correlation method, our approach is much more robust, especially for datasets with sparse localization points.

SMLM represents a significant advancement in microscopy, breaking through the diffraction limit of light to achieve resolution beyond traditional optical microscopy [1,2]. The essence of SMLM lies in capturing tens of thousands of raw images, relying on the sparse blinking and precise localization of fluorescent molecules. Inevitably, prolonged acquisition time introduces drift between the sample and the imaging system, resulting in artifacts in the reconstructed super-resolution image [3]. Drift correction ensures that the SMLM imaging achieves optimal image quality.

In most proposed methods, drift correction involves two steps: drift estimation and compensation. Drift compensation can be achieved through post-processing [4,5] or active compensation [6,7]. Post-processing involves adjusting the positions of fluorescent molecules after data acquisition, whereas active compensation utilizes a nanoscale positioning stage for real-time stabilization. Active compensation, being hardware-based, adds complexity and cost to the system. However, active compensation methods are more effective to tackle the issue of reduced localization accuracy caused by axial drift. One such method relies on the detection of the reflected laser light at the interface between the glass slide and the sample medium [6]. Any changes in the z-position of the sample lead to variations in the reflected laser spot, which are then detected by a quadrant photodiode (QPD). The QPD generates a position-related voltage signal, which is then used as feedback to the nanoscale positioning stage to compensate for the axial drift of the sample [8,9].

Post-processing methods are commonly employed in lateral drift correction due to their relative ease of implementation. The effectiveness of various post-processing compensation methods fundamentally depends on the accurate estimation of drift. A prevalent approach is to manually add fiducial markers to the coverslip, such as gold nanoparticles [10,11], nanodiamonds [12–14], and fluorescent beads [15,16]. Fiducial markers possess high stability and brightness, making this method highly reliable. However, this technique requires additional sample preparation to ensure that there are sufficient and evenly distributed fiducial markers on the coverslip. Besides, the intense brightness of these markers might reduce the localization precision of adjacent probes [15]. In contrast, label-free drift estimation methods, which leverage the inherent structural features of the sample, effectively circumvent these challenges [17–19]. The drift correction is normally based on the scattered signals recorded by a camera [18]. However, it is often computationally intensive for 3D registration with high accuracy using stacks of 2D images.

Another widely used method is based on single-molecule localization events [4]. This method arranges blinking molecules into uniform time intervals, with each interval generating a subset of super-resolution images. The drift of the sample is calculated by cross-correlating these subsets and then adjusting the position of the single molecule according to the computed drift. However, this method requires a sufficient number of blinking events, as more blinking events generally lead to a more precise drift estimation.

In this paper, we propose a novel 3D drift correction method based on both the reflected and scattered laser light. Our method simultaneously achieves focus stabilization and high-precision lateral drift estimation using just one NIR laser. We tested this

method using imaging data of nuclear pore complexes (NPCs) and compared it with the localization events-based method [4]. The results demonstrated that when the number of localization events was sufficient, the precision of our method was nearly identical to the localization events-based method. More importantly, when there were few localization events, our method more accurately corrected the fine structures of the sample, whereas the localization events-based drift correction failed.

In this work, we performed SMLM imaging at room temperature using a custom-built microscope. The scheme of the optical setup is shown in Fig. 1. We used a laser box and a single-mode fiber to illuminate the sample, as described in our previous work [20]. The excitation laser was reflected by a dichroic mirror (Di01-R405/488/561/635, Semrock) before focusing on the objective back focal plane for super-resolution imaging. Fluorescence emitted from the sample was collected by a high NA objective (NA 1.5, UPLAPO 100XOHR, Olympus) and then filtered by a quad-band emission filter (NF03-405/488/561/635E, Semrock). After the tube lens (SWTLU-C, f=180 mm, Olympus), a band-pass filter (ET685/70m, Chroma) was inserted into the beam path to reject residual laser light. Finally, images are acquired by an sCMOS camera (Dhyana 95 V2, TUCSEN) with a pixel size of 11 μm × 11 μm. In addition, a plano-convex cylindrical lens (LJ1516L1-C, Thorlabs) was placed in front of the camera for astigmatism 3D imaging.

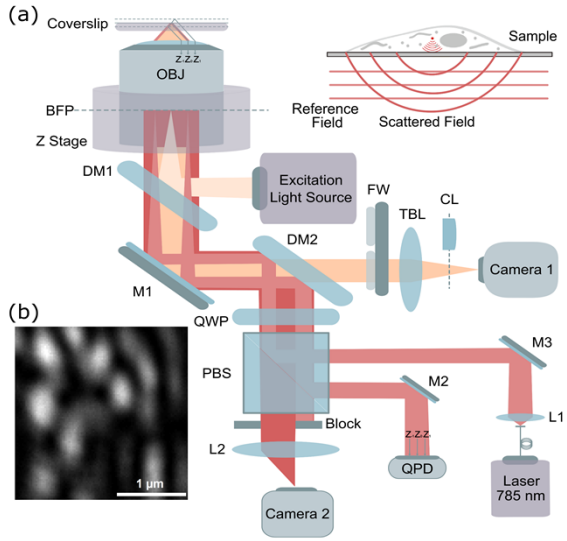

Fig. 1. Schematics of the optical setup for simultaneous acquisition of single-molecule and speckle data. (a) Detailed layout of the optical setup. (OBJ: objective lens, BFP: back focal plane, DM: dichroic mirror, M: mirror, FW: filter wheel, TBL: tube lens, CL: cylindrical lens, QWP: quarter-wave plate, PBS: polarized beam splitter, QPD: quadrant photodiode, L: lens). (b) Speckle pattern of a cell sample.

Light from an ultra-compact diode laser with a center wavelength of 785 nm (iBEAM-SMART-785-S, 125 mW, TOPTICA) is first coupled into a fiber patch cord (OK-678, SM/PM/APC NA=0.12, MFD=4.8 μm, TOPTICA) by the fiber coupler (Smartdock, TOPTICA). Then, the laser emitted from the fiber is collimated by an achromatic doublet lens (f=10 mm) mounted in the rotating adjustable lens tube and kinematic mounts, which can enable us to adjust the polarization direction and the incident angle of 785 nm light to optimize the collection of the light reflected from the glass slide. The 785 nm light is then reflected by a dichroic mirror (FF750-SDi02-25x36, Semrock) and focused at the back focal plane of the objective. A combination of a polarization beam splitter (PBS) with a quarter-wave plate (WPQ10M-780, Thorlabs) is employed to separate the signal light from the incident light. In one direction of the PBS, the reflection beam from the coverslip (CG15XH, Thorlabs) was detected by a quad photodiode array (QP50-6SD2, First Sensor Inc.), whose position-dependent output voltage changes with the distance between the objective and the coverslip. The output voltage of QPD was then connected to the objective z stage controller (E-709.1C1L, Physik Instrumente). With the help of the external sensor mode of the objective z stage (P-725.1CDE2, Physik Instrumente), we can accurately control and lock the axial direction between the objective and the coverslip. In another direction of the PBS, the reflection beam and stray light are blocked by a slit (SP60, Owis). A lens with a focal length of 250 mm collects the scattered light produced by the coverslip surface and the sample. Finally, speckle images, such as the one shown in Fig. 1(b), are acquired by a CMOS camera (CS165MU1/M, Thorlabs) with an optional absorptive neutral density filter.

The software control of the microscope was integrated into Micro-Manager with EMU [21]. The exposure of the two cameras and the excitation light were synchronized under the control of the Micro-FPGA [22]. Typically, we acquired 50,000-100,000 frames with a 20 ms exposure time in the fluorescence channel for super-resolution image reconstruction. In the speckle image channel, triggered by the exposure signal of the fluorescence channel camera, we collected one speckle image for every 16 frames of single-molecule images. Usually, we collected 3,000-7,000 speckle frames, which were used to estimate the lateral drift.

Images obtained in interferometric scattering microscopy exhibit random speckle patterns [23,24]. However, these seemingly irregular patterns contain the position information of the sample. Lin et al. reported that speckle patterns originate from the undulations of the sample and the slide and can serve as optical fingerprints to extract lateral displacement with nanometer precision [25]. Building upon this method, we have improved by using a NIR laser (785 nm) through a PBS to simultaneously achieve speckle pattern generation of the sample and axial focus locking. When the lateral drift occurs in the sample, the speckle pattern also shifts. Within a small range, these patterns are translational invariant. Therefore, we used the sub-pixel registration algorithm proposed in Ref. [26] to estimate the lateral drift from a series of speckle images precisely and then adjusted the positions of the single molecules according to the computed drift.

In the axial direction, we utilized a 785 nm laser, a QPD, and a nanoscale positioning stage to realize active drift correction, which is also known as the focus stabilization system. This technique is based on the positioning of the reflected laser beam. Therefore, it doesn't need to record images to estimate the axial drift. When conducting SMLM experiments, we first need to activate the focus stabilization system.

Our method incorporates axial active focus stabilization, complemented by lateral drift compensation through the post-processing of speckle images. Therefore, the primary task is to demonstrate that our system can achieve long-term focus stabilization, at least meeting the data acquisition time for SMLM imaging, typically ranging from a few minutes to several tens of minutes. We acquired 40,000 frames of bead samples on the sCMOS

camera at a frame rate of 10 Hz with and without the axial focus stabilization system activated. Each round of acquisition took about an hour, thus covering most single-molecule data acquisition durations. Then, we employed the cubic spline method [27] to fit the axial position of the beads in each frame using the calibrated spline PSF, thereby demonstrating the performance of our focus stabilization system (Fig. 2). Fig. 2(a) illustrates the axial position fluctuation of the fluorescent beads over a period of 60 minutes. Without active compensation in the axial direction, the sample drifted about 250 nm in the axial position. After active compensation, the axial drift was effectively minimized. The standard deviation of the axial position of beads over one hour was only 4.6 nm, as shown in Fig. 2(b).

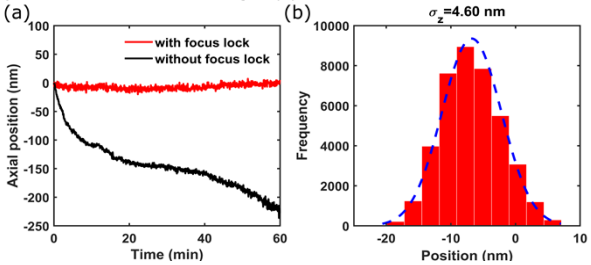

Fig. 2. Performance of the axial active focus stabilization system. (a) The axial position of the sample over 60 min with (red curve) and without (black curve) the focus stabilization system activated. (b) Histogram of the sample positional fluctuations in the axial direction with focus stabilization system activated (std=4.60 nm).

Another pivotal aspect of our method is the estimation of lateral drift based on the speckle images. We assumed that the speckle pattern, to a certain extent, maintains the translational invariance within a small region. Thus, we can use cross-correlation algorithms to obtain the lateral drift from a series of speckle images. Drift estimation based on fluorescent beads has been proven to be highly accurate and served as a reference. To validate our drift estimation method, we concurrently captured fluorescence and speckle images of beads. Then, we computed their respective drifts for comparison, as shown in Fig. 3.

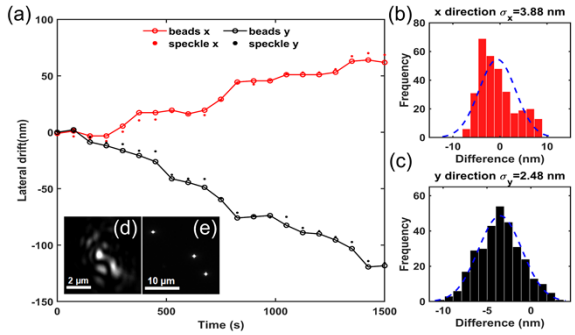

Fig. 3. Comparison of drift estimation between fluorescence images and speckle images. (a) Lateral drift measurement in fluorescence and speckle images. (b-c) Differences between beads-based and speckle-based drift estimation in the lateral direction are shown, with the blue dashed lines indicating the histogram fitting with a normal distribution. (d-e) Simultaneously acquired speckle pattern and fluorescent beads image.

Fig. 3(a) shows the lateral drift estimated from both fluorescent bead images and speckle images using the same cross-correlation algorithm. We further analyzed the differences in lateral drift estimation between the two methods in Fig. 3(b) and (c). From Fig. 3(b) and (c), we can conclude that the differences in the lateral direction between the two methods are generally within 5 nm. Fig. 3(d) and (e) show the raw images of fluorescent beads and the speckle pattern.

So far, we have successfully validated the capabilities of our method in both the axial and lateral directions. We then further verified the performance of our system in practical 3D SMLM imaging using cell samples, with single-molecule localization and image rendering performed using SMAP [28]. Additionally, we compared its performance with that of the localization events-based drift correction method. For the methods of sample preparation and labeling, please refer to our previous work [29], with details described in Supplement 1.

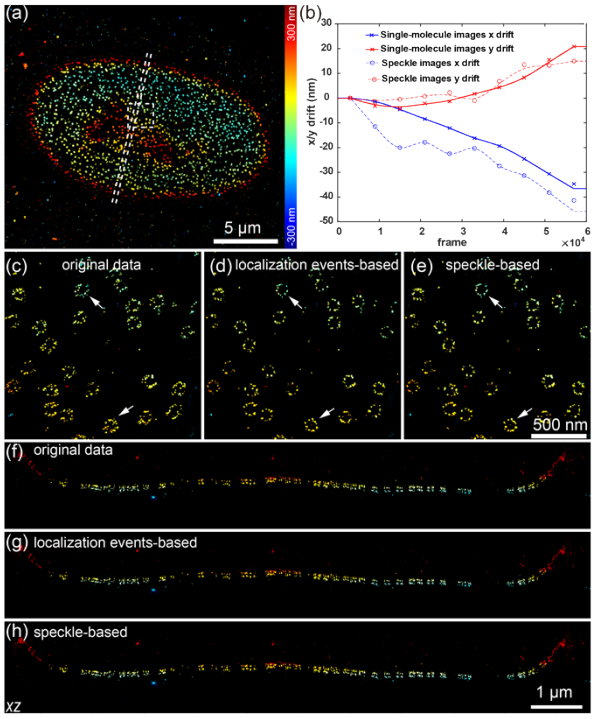

Fig. 4. Comparison between localization events-based and speckle-based 3D drift correction. (a) Reconstructed image of the entire field of view (FOV). (b) The estimated drifts by the two methods. (c-e) Magnified area of the box in a, showing (c) the original data with drift, (d) the data corrected by the localization events-based method, and (e) the data corrected by the speckle-based method. (f-h) The side-view cross-section of the region is indicated by the dashed line in (a), which corresponds to the double-ring structure of the NPC in the three scenarios.

Fig. 4(a) shows the reconstructed 3D image of the U2OS cell nucleus, with many NPCs distributed on the nucleus membrane. As shown in Fig. 4(b), the lateral drift difference between our method and localization events-based method is only a few nanometers. Both methods effectively corrected the drift in the original data, and the final reconstructed images are almost the same [Fig. 4(d-e)]. The double-ring structure of NPCs, displayed in the XZ plane in Fig. 4(f-h), is clearly distinguishable, with almost no noticeable changes before and after drift correction. This indicates that our focus stabilization system could maintain axial stability during data acquisition. These results demonstrate that the precision of our

speckle image-based drift correction method is compatible with SMLM images with a few tens nanometer resolution.

Finally, we performed 3D SMLM imaging of the NPC in the equatorial plane of the nucleus. The drift correction results of the localization events-based method and our speckle image-based correction method are shown in Fig. 5. The NPCs located on the equatorial plane of the nucleus formed two lines in the top view image [Fig. 5(a)], where the number of localization events was significantly lower than that on the upper and lower surfaces of the cell nucleus. Drift correction based on localization events heavily relies on the number of localization points in the dataset. Sparse localization points may lead to imprecise drift estimation, resulting in a significant difference in lateral drift estimation between the localization events-based method and our speckle-based method [Fig. 5(b)].

Fig. 5(c-e) shows the magnified area of the double-ring in Fig. 5(a). Before drift correction, the double-ring structure is not very clear [Fig. 5(c)]. Furthermore, we found that the localization events-based method often failed to accurately correct the equatorial data of NPCs due to sparse localizations [Fig. 5(d)]. The two-line structure is often mixed with each other. In contrast, data corrected using our method can reconstruct a more distinct double-ring structure [Fig. 5(e)]. It indicates that the performance of the speckle-based 3D drift correction method is independent of the density of the localization events and, thus, more robust to different biological samples.

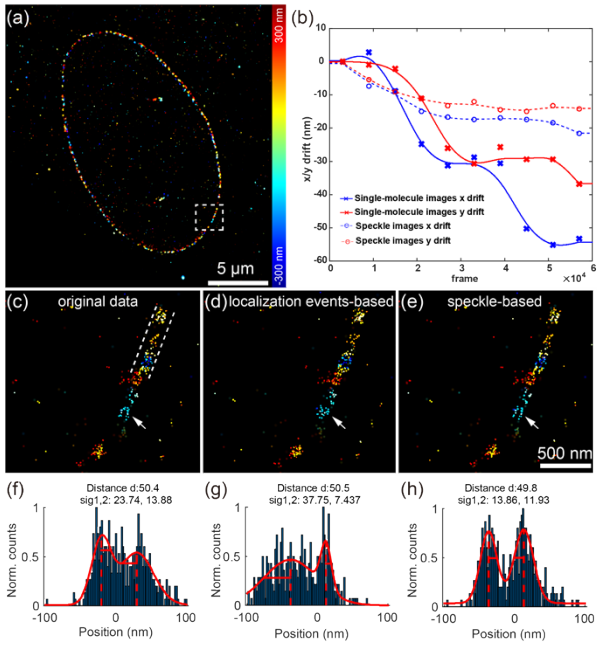

Fig. 5. Comparison between localization events-based and our speckle-based 3D drift correction in the dataset with sparse localization events. (a) Reconstructed image of the entire FOV. (b) Drift estimated by the two methods. (c-e) Magnified area of the boxed region in (a), showing (c) the original data with drift, (d) the data corrected by the localization events-based method, and (e) the data corrected by our speckle-based method. (f-h) Intensity profile along the white dashed lines in c-e.

In summary, we have developed a novel 3D drift correction method for SMLM based on speckle images and reflected NIR detection. We used one NIR laser to illuminate cell samples, achieving active focus stabilization by compensating the z-piezo stage displacement using the reflected laser position monitored by QPD. Simultaneously, the speckle pattern generated by the NIR laser is used for lateral drift estimation. In this work, we validated the high precision of drift estimation based on speckle images, which was comparable to the localization events-based method when sufficient single-molecule localization data was collected. Additionally, we demonstrated that without sufficient localization events, our method exhibited superior correction performance compared to the localization events-based method. We expect that our method offers a new solution for accurate 3D drift correction compatible with super-resolution imaging. In the future, by replacing the post-processing strategy in the lateral direction with active XY stage control, our system could be able to achieve real-time active 3D drift correction using a single laser light.

Funding. National Natural Science Foundation of China (62375116); Shenzhen Medical Research Fund (B2302038); Key Technology Research and Development Program of Shandong (2021CXGC010212); Shenzhen Science and Technology Innovation Commission (KQTD20200820113012029, JCYJ20220818100416036); Startup Grant from Southern University of Science and Technology.

Disclosures. Yiming Li has a pending Chinese patent(202310158216X).

Data availability. Data underlying the results presented in this paper are not publicly available at this time but may be obtained from the authors upon reasonable request.

Supplemental document. See Supplement 1 for supporting content.

References

1. M. J. Rust, M. Bates, and X. Zhuang, Nat. Methods **3**, 793 (2006).
2. E. Betzig, G. H. Patterson, R. Sougrat, *et al.*, Science **313**, 1642 (2006).
3. S. Coelho, J. Baek, J. Walsh, *et al.*, Nat. Protoc. **16**, 497 (2021).
4. Y. Wang, J. Schnitzbauer, Z. Hu, *et al.*, Opt. Express **22**, 15982 (2014).
5. J. Cnossen, T. J. Cui, C. Joo, *et al.*, Opt. Express **29**, 27961 (2021).
6. S. A. Jones, S. H. Shim, J. He, *et al.*, Nat. Methods **8**, 499 (2011).
7. R. McGorty, D. Kamiyama, and B. Huang, Opt. Nanoscopy **2**, 3 (2013).
8. P. Annibale, M. Scarselli, M. Greco, *et al.*, Opt. Nanoscopy **1**, 9 (2012).
9. V. Navikas, A. C. Descloux, K. S. Grussmayer, *et al.*, Nanophotonics **10**, 2451 (2021).
10. G. Grover, W. Mohrman, and R. Piestun, Opt. Express **23**, 23887 (2015).
11. H. Ma, J. Xu, J. Jin, *et al.*, Biophys. J. **112**, 2196 (2017).
12. J. Yi, A. Manna, V. A. Barr, *et al.*, Mol. Biol. Cell **27**, 3591 (2016).
13. W. Colomb, J. Czerski, J. d. Sau, *et al.*, J. Microsc. **266**, 298 (2017).
14. A. Balinovic, D. Albrecht, and U. Endesfelder, J. Phys. D: Appl. Phys. **52**, 204002 (2019).
15. P. J. Zessin, C. L. Krüger, S. Malkusch, *et al.*, Opt. Nanoscopy **2**, 4 (2013).
16. K. Li, J. Ni, X. Tan, *et al.*, Opt. Express **31**, 26764 (2023).
17. S. Coelho, J. Beak, M. S. Graus, *et al.*, Sci. Adv. **6**, eaay8271 (2020).
18. S.-Y. Chen, R. Heintzmann, and C. Cremer, Biomed. Opt. Express **10**, 6462 (2019).
19. X. Fan, T. Gensch, G. Büldt, *et al.*, Opt. Express **28**, 32750 (2020).
20. S. Fu, M. Li, L. Zhou, *et al.*, Opt. Lett. **47**, 3031 (2022).
21. J. Deschamps and J. Ries, BMC Bioinf. **21**, 456 (2020).
22. J. Deschamps, C. Kieser, P. Hoess, *et al.*, HardwareX **13**, e00407 (2023).
23. J.-S. Park, I.-B. Lee, H.-M. Moon, *et al.*, Chem. Sci. **9**, 2690 (2018).
24. R. W. Taylor, R. G. Mahmoodabadi, V. Rauschenberger, *et al.*, Nat. Photonics **13**, 480 (2019).
25. S. Lin, Y. He, D. Feng, *et al.*, Phys. Rev. Lett. **129**, 213201 (2022).
26. M. Guizar-Sicairos, S. T. Thurman, and J. R. Fienup, Opt. Lett. **33**, 156 (2008).
27. Y. Li, M. Mund, P. Hoess, *et al.*, Nat. Methods **15**, 367 (2018).
28. J. Ries, Nat. Methods **17**, 870 (2020).
29. S. Fu, W. Shi, T. Luo, *et al.*, Nat. Methods **20**, 459 (2023)